Microdomain Transformations in Mosaic Mesocrystal Thin Films

*Yuan Jiang, Haofei Gong, Maciej Grzywa, Dirk Volkmer, Laurie Gower, and Helmut Cölfen**

An easy design route via simple evaporation is reported for macroscopic mosaic thin films comprising the quaternary system of DL-lysine·HCl, poly(acrylic acid), water, and EtOH. By depositing droplets of the quaternary dispersions onto hydrophilic cover slips, the formation of macroscopic crack-free mosaic mesocrystal thin films are produced. The formation follows a multistage crystallization process, which includes the formation of a polymer-induced liquid-precursor (PILP) phase, the formation of spherulitic thin films, and the recrystallization of mosaic mesocrystal thin films. A slow cooling rate is noted to be beneficial for the mesocrystal thin films, enabling the films to be crack-free and to display low surface roughness at the nanoscale.

1. Introduction

Bio-inspired crystallization is an effective way for the preparation of functional materials with various forms and functions.[1] The preparation of such materials relies on additives such as polyelectrolytes, which are mimics of highly acidic or basic proteins—key players necessary for controlling the nucleation of biominerals and their final morphology.[2–5] The preparation of bio-inspired crystalline thin films usually requires one extra component, a substrate. Insoluble macromolecular matrices, which are the substrates in biomineralization, have been suggested to induce nucleation at certain positions, confining the crystallization within a compartment and controlling the orientation of thin films.[2,3,6] Supramolecular assemblies, such as self-assembled monolayers (SAMs),[7–10] Langmuir monolayers,[11–13] and macromolecular thin films,[14–19] have been applied to mimic insoluble matrices in biomineralization in order to control the growth of inorganic–organic hybrid thin films; this has resulted in various forms of thin films. Xu et al. pioneered the preparation of $CaCO_3$ thin films using a porphyrin-containing monolayer as the matrix, and continuous thin films were obtained with nanoparticles as the building blocks.[11] Since then, a large number of in vitro studies on mineralization systems have been carried out following a multistage crystallization route, e.g., the formation of amorphous $CaCO_3$ or calcium phosphate (CaP) nanoparticles in solution, the adsorption of the nanoparticles onto the matrix, and the fusion of nanoparticles into mosaic or single-crystalline patterns.[20–22] A special feature of biomimetic thin films is that they can consist of building blocks of crystallographically ordered nanoparticles, leading to single-crystalline properties within the film. The term "mesocrystal," which is an abbreviation for "mesoscopically structured crystal," has been used to describe nanoparticle superstructures with mutual crystallographic order and often single-crystalline properties.[23–28] Although an insoluble polymer matrix is indispensible in biomineralization, the biomimetic thin films of several well-studied cases were prepared directly on a bare hydrophilic surface via a multistage crystallization route without any pre-existing matrix, which addresses the importance of physicochemical factors in biomimetic routes[20,29–33] as well as in biomineralization.[2]

Evaporation is an effective way to produce patterned thin films on various substrates.[29,34,35] Thin films are obtainable when the solute–substrate interaction is stronger than the substrate–solvent and the solute–solvent interactions.[36] Various solutes such as supramolecules,[37] macromolecules,[38,39] and nanoparticles[40–44] can also be shaped into patterned structures, where the key factor is the processing route; however, patterned thin films with mutually oriented nanoparticles obtained using evaporation have rarely been reported. A notable exception is the work of Ahniyas et al., who have shown that additional external fields such as magnetic fields can be utilized to order nanoparticles in a thin film with a superlattice structure.[44] Typically, processing parameters, such as temperature, humidity, particle concentration, and cooling rate, have enormous influences on microscopic even macroscopic patterns.[45] Two suitable ways, namely spin-coating and dip-coating, have been employed for the preparation of homogeneous liquid thin layers at the macroscale. Spin-coating has a characteristically

Dr. Y. Jiang,[+] Prof. H. Cölfen,[++]
Max Planck Institute of Colloids and Interfaces
Colloid Chemistry, Am Mühlenberg
D-14476 Golm, Germany
E-mail: helmut.coelfen@uni-konstanz.de
Dr. H. Gong, Dr. M. Grzywa, Prof. D. Volkmer
Institute of Physics, Chair of Solid State & Materials Chemistry
Augsburg University
D-86159 Augsburg, Germany
Prof. L. Gower
Materials Science & Engineering, University of Florida
Gainesville, FL 32611, USA
[+]Present address: Department of Chemical Engineering, Massachusetts Institute of Technology, 77 Massachusetts Ave., Cambridge, MA 02139, USA
[++]Present address: Physical Chemistry, University of Konstanz, D-78457 Konstanz, Germany

fast evaporation rate, always resulting in non-continuous crystalline domains. On the other hand, dip-coating has the advantage of a slow evaporation rate, and is preferred for the synthesis of continuous ceramic thin films, for instance.[29,34,35]

The surface properties of a template also have a tremendous influence on the form of the resulting biomimetic thin films. For example, Cho and co-workers indicated that continuous amorphous $CaCO_3$ thin films were obtained on various polymeric substrates[15] as well as on bare silicon and mica surfaces.[31] They found that inhibitory substrates alone (without polyanionic additive) could also lead to amorphous calcium carbonate films, but only under conditions of high supersaturation.[31] In addition, a surface energy effect has also been observed elsewhere; by choosing various polymer modifications on inhibitory substrates, different morphologies such as hemispheres and thin films have resulted.[32] In the polymer-induced liquid-precursor (PILP) route, it was found that $CaCO_3$ precursor droplets could be selectively deposited on anionic SAMs rather than on hydrophobic ones, and the amorphous-to-crystalline transformation was also found to be markedly higher in the anionic SAMs.[10] To form a calcium carbonate PILP phase, micromolar quantities of short-chained polyanionic polyelectrolytes, such as poly(aspartic acid), are added to the mineralizing system to sequester the mineral cations and corresponding anions, along with their hydration waters. Liquid–liquid phase separation occurs, forming metastable PILP droplets rich in solute, which was recently found to result from the stabilization of a liquid condensed phase for $CaCO_3$[46] rather than from the possible crosslinking of stable prenucleation clusters.[47,48] Subsequently PILP droplets coalesce into a continuous thin film on a substrate. Finally, solidification and crystallization occur to form a mosaic thin film containing single-crystalline domains of crystallographically ordered coalesced nanoparticles.[10]

The PILP route towards crystalline bulk phases and coatings has been reported for the preparation of microspheres of small organic molecules, such as charged amino acids[49,50] and pigments,[51] with nanoparticles as building blocks, as well as for the preparation of hierarchical mesocrystal thin films, with nanoparticles as building blocks.[52] Herein, we extend the PILP route previously used for the preparation of microspheres to the fabrication of mosaic mesocrystal thin films. Droplet deposition as a modified form of the dip-coating method is combined with an evaporation-induced self-assembly process for the preparation of mesocrystalline DL-lysine·HCl (DL-Lys·HCl) thin films at the macroscale with poly(acrylic acid) (PAA) as an additive. Solvent evaporation plays a key role in the deposition of a continuous spherulitic thin film on the substrate. Subsequently, a mosaic mesocrystalline thin film is formed via the spherulitic phase (**Scheme 1**). The morphology and crystal structure of the final mosaic thin films for various process parameters, such as temperature, $m_{\text{DL-Lys·HCl}}/m_{\text{PAA}}$ (the mass ratio of DL-Lys·HCl and PAA), the concentration of DL-Lys·HCl, and $V_{\text{EtOH}}/V_{\text{aq}}$ (the volume ratio of EtOH and the aqueous solution of DL-Lys·HCl and PAA), were investigated. High-quality thin films can be prepared when employing a relatively slow cooling rate.

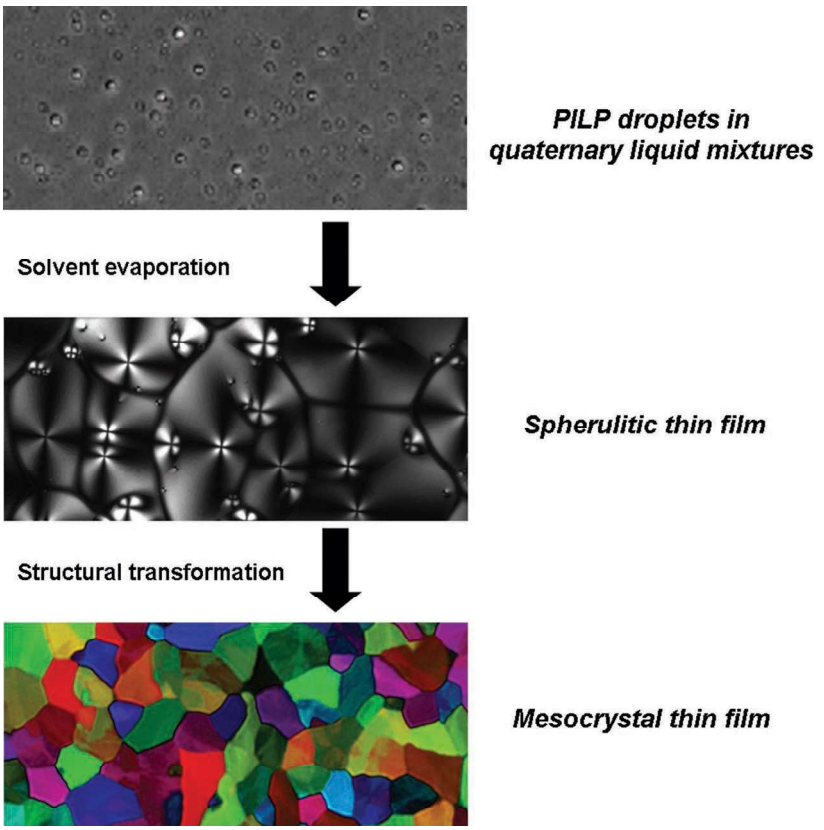

Scheme 1. The entire transformational process under (polarized) optical microscope.

2. Results

2.1. Multistage Crystallization

The multistage crystallization process starts from an evaporation process in an open vessel. When an aqueous solution of DL-Lys·HCl and PAA mixed with EtOH, the mixture becomes turbid. Metastable liquid droplets form immediately by a liquid–liquid phase separation because EtOH constitutes a nonsolvent for DL-Lys·HCl and PAA. Metastable droplets of several micrometers in size are shown in the optical microscopy (OM) images in **Figure 1**A. Within ~1 min, the droplets begin to redissolve upon continuous evaporation of the solvent. A homogeneous liquid layer forms within ~2 min thereafter (Figure 1B). This phenomenon can be explained by the different evaporation rates of water and EtOH in the water–EtOH mixture because the evaporation rate of EtOH is much faster than that of water. As the water content of the liquid phase increases steadily, the precipitated DL-Lys·HCl becomes

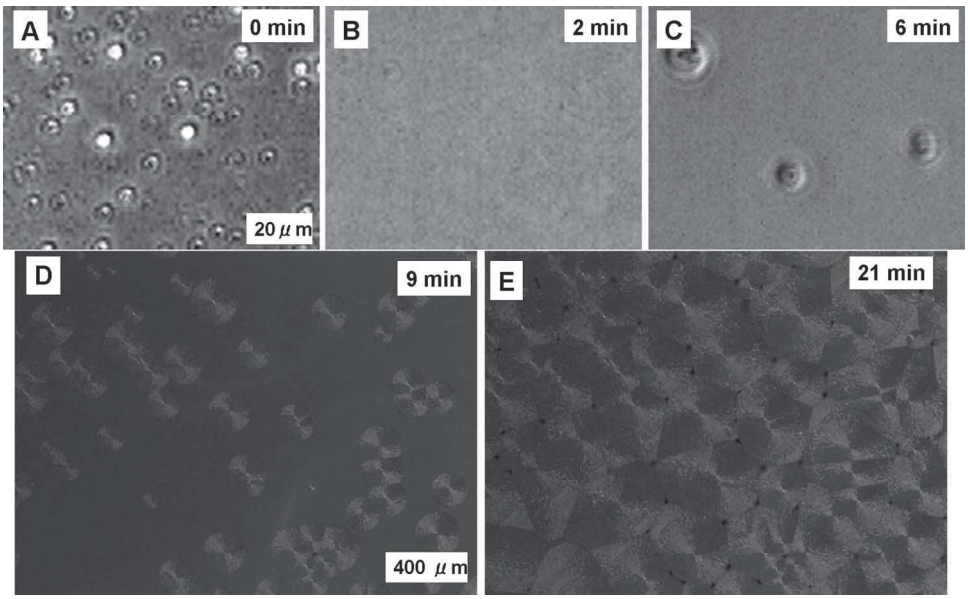

Figure 1. A–C) Optical microscopy (OM) images show the disappearance of PILP droplets within the solution phase followed by the formation of spherulites on the hydrophilic cover slip. D,E) Polarized OM (POM) images show the growth of spherulites on the cover slip. The same position and the same magnication was used for A–C and for D and E.

soluble, and after ~2 min, a homogeneous liquid solution layer is observed in the OM image. Further solvent evaporation leads to spherulite formation because of a surface nucleation process that is far from equilibrium;[53] the nucleation starts ~6 min after the droplet deposition step (Figure 1C). The spreading of spherulites (Figure 1D,E) takes approximately another 15 min, resulting in the formation of a uniform and continuous coating on top of the cover slip. Spherulites are ~100–200 μm in size with a wide size distribution (Figure 1E). The evaporation process is a prerequisite for the formation of a continuous thin film on top of a hydrophilic cover slip. For comparison, macroporous microspheres were obtained via these liquid droplets in a closed system; these results have been reported elsewhere.[49,51,52]

2.2. Characterization of Thin Films

The quality of hin films is optimized by tuning a series of parameters. Unlike some well-studied biomimetic crystallization cases, where spherulites were the finally obtained crystalline phase,[31] we observed that the continuous spherulitic thin films recrystallized into mosaic thin films in the next 24 h. The as-prepared spherulitic and mosaic thin films were imaged with both OM and polarized OM (POM). **Figure 2**A shows a representative OM image of a spherulite thin film (sample G in **Table 1**, $V_{EtOH}/V_{aq} = 5$).

To precisely clarify whether the same orientation was preserved after recrystallization of the spherulitic thin films to the mosaic thin films, the quantitative birefringence microscopic technique was applied to scan the transformation during the recrystallization process. This technique measures the retardance magnitude at every pixel of a charge-coupled device image; therefore, it can provide quantitative orientation information of each domain. Figure 2B shows that single-crystalline domains start to grow sporadically within the spherulitic pattern, which is indicative of heterogeneous nucleation on the spherulite matrix. A majority of single-crystalline domains (see circles 1, 3, 4, and 5) follow the orientation of the spherulitic matrix, as indicated by their identical color; different colors represent different orientations of domains. However, there exist several domains that show a different orientation from the spherulitic matrix (circle 2 in Figure 2B, for example). The orientation of these domains does not change during their growth (see video in the Supporting Information, "polycrystal transformation at RT.avi"). The quantitative birefringence microscopy images can also provide the orientational distribution of the mosaic domains in each spherulitic pattern. The quantitative birefringence microscopy image in Figure 2C shows a dominance of dark color or lighter color in different quadrants of the mosaic thin film. This phenomenon suggests different orientational preferences of the mosaic domains in the different quadrants.

Time-resolved atomic force microscopy (AFM) was applied to detect possible morphological changes during the formation of the spherulitic thin films. The result shows that nanoparticles exist in the initially formed spherulitic thin films, and that there is no topological change on the surface thereafter (see the Supporting Information, Figure S1). The X-ray diffraction (XRD) pattern shows the existence of several peaks (Supporting Information, Figure S2) in the initially formed spherulitic thin film, which suggests that the film is poorly crystalline.[54] The spherulitic thin film crystallizes with time into a mosaic mesocrystal thin film.

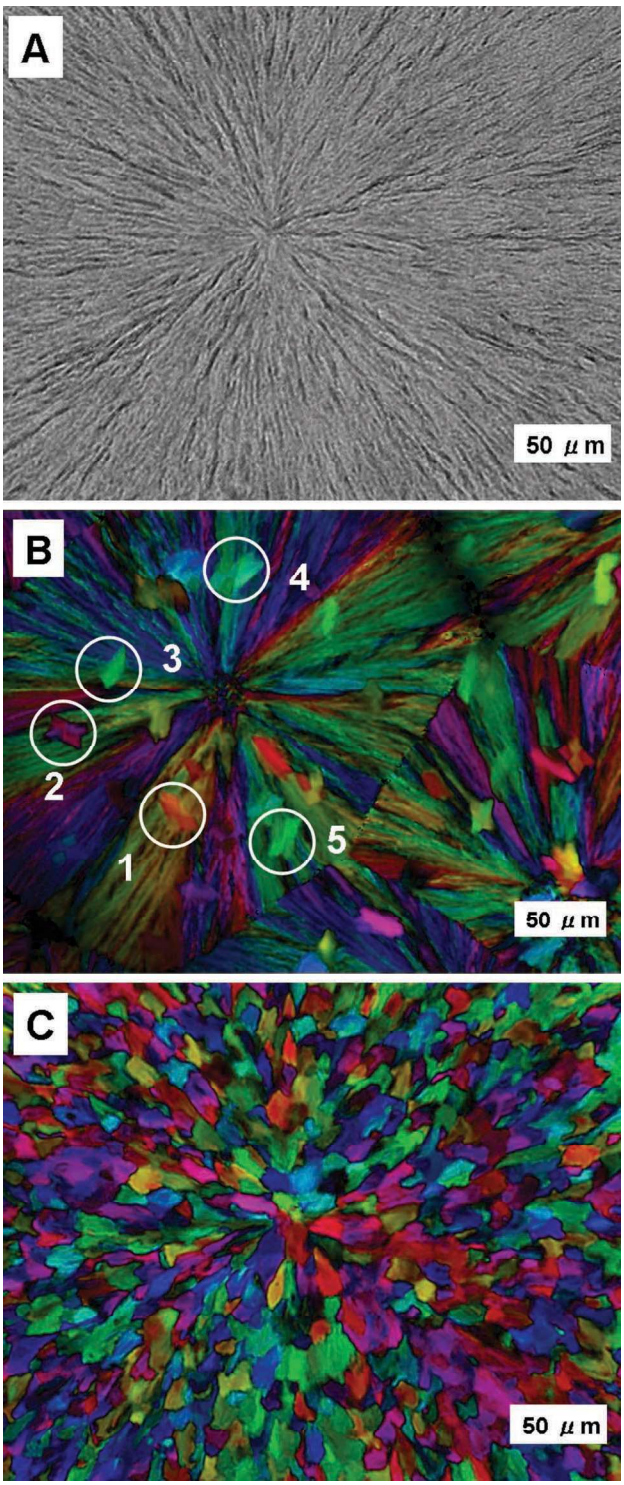

Figure 2. A) OM image of the as-formed mosaic thin film (sample G; V_{EtOH}/V_{aq} = 5). B) Quantitative birefringence microscopy image during the transformation from spherulitic to mosaic thin film at ~5 h. Some growing single-crystalline domains are indicated within white circles (sample G; V_{EtOH}/V_{aq} = 3). C) Quantitative birefringence microscopy image of the as-formed mosaic thin film. In quantitative birefringence microscopy images, the orientation preference of different domains is shown as different colors (sample G; V_{EtOH}/V_{aq} = 5).

Table 1. The compositions of the aqueous solutions for the preparation of the thin films.

Sample code	[DL-Lys·HCl] [g·L^{-1}]	[PAA] [g·L^{-1}]
C	70	7
G	70	3.5
M	70	14

2.3. Compositional and Processing Optimization

First, the indispensible existence of PAA and EtOH is considered. A reference experiment was performed by dipping the cover slip into a mixture of DL-Lys·HCl aqueous solution and EtOH, and only isolated crystals that were hundreds of micrometers in size were obtained (Supporting Information, Figure S3A). Such single-crystals follow the classical crystallization route via molecular attachment; therefore, PAA is an indispensible ingredient for the preparation of mosaic thin films covering the whole surface, where it inhibits or slows down the growth rate of DL-Lys·HCl single-crystals while inducing the PILP droplets.

EtOH is an evaporating solvent with good wetting behavior on the hydrophilic glass surface. A comparison experiment was performed by dipping the slide into a DL-Lys·HCl–PAA aqueous solution, and only isolated particles composed of micrometer-sized crystals were obtained (Supporting Information, Figure S3C). This result suggests that the existence of EtOH is essential for depositing solute homogeneously on the substrate, indicating that a continuous thin film is made possible by the low surface tension of EtOH.

Parameters such as [DL-Lys·HCl], [PAA], $m_{DL\text{-}Lys\cdot HCl}/m_{PAA}$, and V_{EtOH}/V_{aq} were also investigated to improve the quality of the as-prepared thin films. The compositions of the aqueous solutions are summarized in Table 1 and **2**. These aqueous solutions were mixed with EtOH at various values of V_{EtOH}/V_{aq} for the preparation of mesocrystalline thin films (**Table 3**). First, various DL-Lys·HCl–PAA aqueous solutions were mixed with EtOH at V_{EtOH}/V_{aq} = 9. Mosaic thin films are reliably obtained with aqueous solutions B or C (Table 2). Thin films from the more diluted sample A only show weak birefringence signals under POM. We attribute this to the fact that the solute is not densely packed in this case and that the driving force of crystallization is weak. On the other hand, the co-existence of

Table 2. The compositions of aqueous solutions where $m_{DL\text{-}Lys\cdot HCl}/m_{PAA}$ is at 10/1. The morphology of the thin films is determined by keeping V_{EtOH}/V_{aq} at 5.

Sample code	[DL-Lys·HCl] [g·L^{-1}]	[PAA] [g·L^{-1}]	Morphology of resulting thin film
A	30	3	Mosaic, weak contrast in POM
B	50	5	Mosaic, good contrast in POM
C	70	7	Mosaic, good contrast in POM
D	100	10	Mosaic with some micro-spheres on the surface

Table 3. Morphologies of thin films formed by mixing sample C with EtOH at various ratios of V_{EtOH}/V_{aq}.

V_{EtOH}/V_{aq}	Morphology
>9	Amorphous
7	Mesocrystal
5	Mesocrystal
3	Mesocrystal
2	Mesocrystal with cracks
1	Mesocrystal with cracks

microspheres and a mesocrystalline thin film is observed by mixing sample D with EtOH. The high solute content in the aqueous solution causes a high supersaturation of DL-Lys·HCl in the quaternary mixture; therefore, the driving force for the formation of microspheres, which occurs from direct crystallization in the PILP droplets, is so high that microspheres are formed directly within the mixture before they fall on the substrate.[50]

Next, the effect of varying the $m_{DL\text{-}Lys\cdot HCl}/m_{PAA}$ ratio was investigated by keeping the value at 5, 10, or 20, as summarized in Table 1. Mosaic thin films are obtained when $m_{DL\text{-}Lys\cdot HCl}/m_{PAA}$ is at 10 or 20. On the other hand, spherulitic thin films are stabilized against transformation into mosaic thin films when $m_{DL\text{-}Lys\cdot HCl}/m_{PAA}$ is 5. We propose that the high content of PAA in the thin film increases the recrystallization barrier between the spherulitic form and mosaic form (Supporting Information, Figure S3B).

The value of V_{EtOH}/V_{aq} is also an important parameter for the quality of the mosaic thin films (Table 3). The morphology of thin films formed by mixing sample C with EtOH at various values of V_{EtOH}/V_{aq} were noted. When $V_{EtOH}/V_{aq} \geq 9$, a weak birefringence contrast exists in polarized light, suggesting that the thin films are poorly crystalline due to the fast precipitation. On the other hand, thin films with cracks are obtained when V_{EtOH}/V_{aq} is between 1 and 2. We attribute this to the high solute content resulting in an increased thickness of the films, causing a large strain during the drying process. High-quality mosaic thin films are only obtainable when the values of V_{EtOH}/V_{aq} are between 3 and 7.

2.4. Cooling Rate

Mosaic thin films prepared at room temperature (RT) are rough in topography (Supporting Information, Figure S4). In addition, the orientation distribution of the single-crystalline domains is nearly reminiscent of the initial spherulitic thin films. It was therefore desired to see if we could prepare mosaic thin films with a flat surface at the nanoscale. To achieve this goal, a cooling process turns out to be a key step.[45] This cooling step is used to tune the properties of mosaic thin films, such as domain size and orientation. The initial evaporation process was performed at 40 °C, and the spherulitic thin film formed was subjected to various cooling rates. The experiments were performed using sample G and $V_{EtOH}/V_{aq} = 5$ as the model system with a cooling rate of 1 °C·h^{-1}.

The structural details of the thin films formed via a slow cooling rate process were first investigated using POM. **Figure 3**A shows that each single-crystalline domain is ~5–20 μm. Unlike the single-crystalline domains prepared entirely at RT, which showed some degree of orientation (Figure 2C), the single-crystalline domains in thin films obtained using a cooling process revealed a more random distribution when investigated using quantitative birefringence microscopy (Figure 3B).

The cooling rate is crucial to the size of the single-crystalline domains in the preparation of mosaic thin films. Two further cooling rates were applied to investigate possible structural changes. In the first route, the cooling rate was decreased at a rate of 0.5 °C·h^{-1}. The resulting thin films showed larger single-crystalline domains of ~10–30 μm in size, and the orientation of the single-crystalline domains is random (Figure 3C). In another route, a spherulitic thin film was cooled down from 40 °C to RT under ambient conditions. Many single-crystalline domains at a size scale of sub-micrometers are formed in the thin film (Figure 3D). A video camera was used to scan the structural changes during the phase transition (see video "fast cooling rate.avi" and Figure S5 in the Supporting Information).

The kinetic information of the mosaic thin film growth was also examined by combining a heating stage with the quantitative birefringence microscopic technique (**Figure 4**). The spherulitic thin film is stable between 50 and 40 °C. At 39 °C, the appearance of three nuclei is detected, which are highlighted in the insets of Figure 4B. The growth of the single-crystalline domains is then scanned at 38 °C (see video "slow cooling rate.avi" in the Supporting Information). The average growth rate of a single-crystalline domain is ~360 nm·min^{-1} at 38 °C. It is difficult to determine the precise rate because the growing nuclei were nonspherical in morphology, which is a result of the strains in various directions parallel to the cover slips being different.

AFM was used to check the structural details of the mosaic thin films at the micro- and nanometer scales. The tree patches in **Figure 5**A are the remnant spherulitic patterns, and each patch is tens of micrometers in size. Each white spot is the nucleation point of a spherulitic pattern during the evaporation process. Compared to the thin films prepared at RT with rough surfaces (Figure S4, Supporting Information), the ones herein are flat at the nanometer scale (within ±5 nm from height analysis, Figure 5C), except for the boundary areas and the nucleation spot (Figure 5A). Each major domain breaks into many single-crystalline domains that are ~5–20 μm in size, as shown in Figure 5B. Figure 5C shows that the building blocks of these domains are tightly packed nanoparticles of ~30 nm in size. To clarify whether the building blocks of mosaic thin films are nanoparticles (not only on the surface), a mosaic thin film was scratched with a knife and characterized using AFM. The AFM image clearly shows that the building blocks are nanoparticles not only on the surface but in the bulk phase of the thin film (Supporting Information, Figure S7). Because the building blocks are nanoparticles, and the nanoparticles within each single-crystalline domain show the same orientation in POM and quantitative birefringence microscopy (Figure 3A–D), the mosaic thin film is an assembly of mesocrystal domains with their surface morphology retaining the surface topology of the spherulitic precursors.

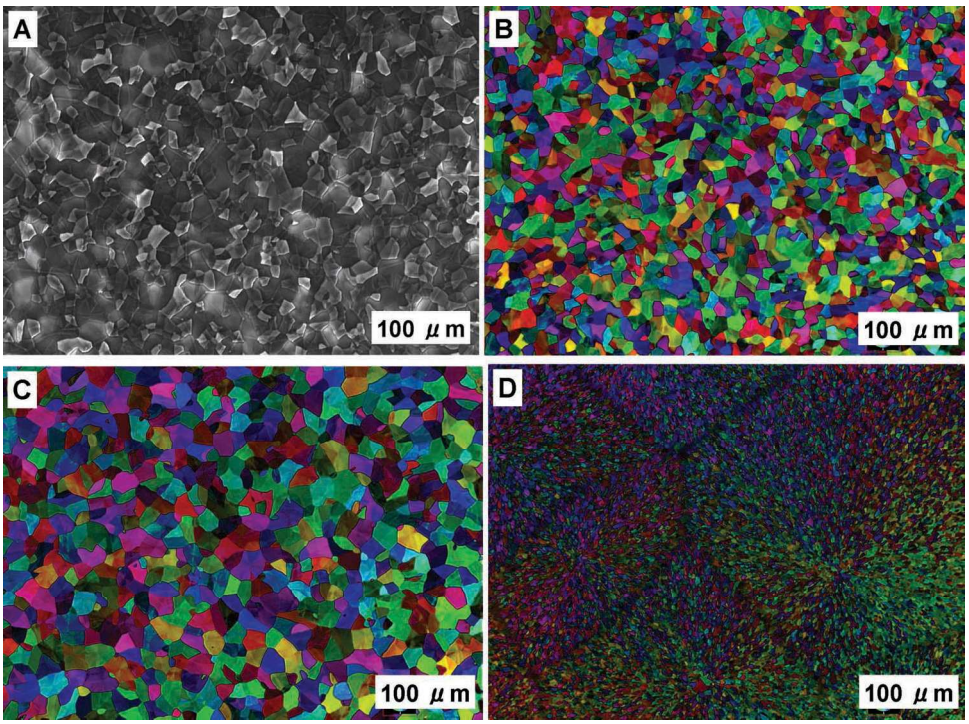

Figure 3. A) POM image, showing a mosaic thin film formed by decreasing the temperature of the sample from 40 °C to RT with a cooling rate of 1 °C·h^{-1}. B) Quantitative birefringence microscopy image of the same sample. C,D) Quantitative birefringence microscopy images, showing the mesocrystal thin films obtained via different cooling processes: cooling rate of 0.5 °C·h^{-1} (C); sample is cooled from 40 °C to RT in an open vessel maintained at RT (D). Sample G; $V_{EtOH}/V_{aq} = 5$).

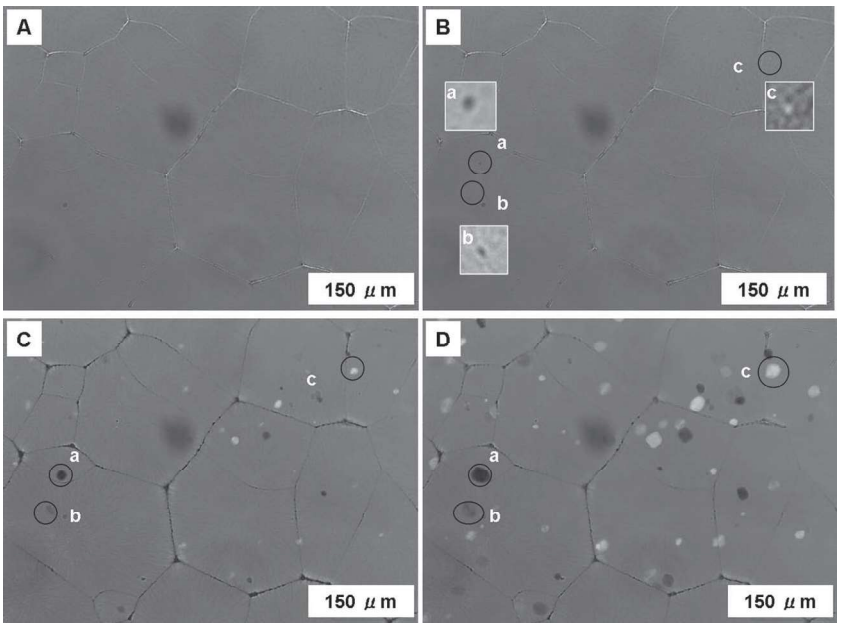

Figure 4. Quantitative birefringence microscopy images showing the nucleation and growth of a mosaic thin film from a spherulitic matrix during a cooling process with a cooling rate of 1 °C·h^{-1}: A) 40, B) 39, C) 38, and D) 38 °C. Sample G; $V_{EtOH}/V_{aq} = 5$. The time each image was taken was A) 0, B) 6, C) 26, and D) 79 min. In B, three nucleation sites are highlighted, and their growth can be followed in C and D. The size of inset images of B is 10 μm. The spherulitic phase is difficult to see because the contrast is relatively low. A representative image showing the co-existence of the spherulitic phase and mosaic structures is provided in the Supporting Information, Figure S6.

2.5. Polymorph Determination

The powder XRD measurement shows a different peak pattern (Supporting Information, Figure S8A) than those known for DL-Lys·HCl (Powder Diffraction File (PDF) 042-1923 and 047-1985; see the pattern for 047-1985 in Figure S9 of the Supporting Information). There are two possibilities to account for this: 1) DL-Lys·HCl in mosaic thin films crystallizes as a distinct polymorph; or 2) DL-Lys·HCl crystallizes into its solvate to show another pseudopolymorph of DL-Lys·HCl, which is not yet described in the literature.

Two experiments have been designed to test the stability of the aforementioned thin films. First, the mosaic thin film was heated to 220 °C (~70 °C below the melting point of DL-Lys·HCl) to examine its stability. The peak positions in the XRD pattern are the same as those recorded from a sample at RT (Supporting Information, Figure S8A,B). Temperatures higher than 220 °C caused partial decomposition of the thin film; thus, this method is not conclusive for excluding the possible existence of a pseudopolymorph of DL-Lys·HCl because the solvent molecule attached to DL-Lys·HCl may detach at temperatures above

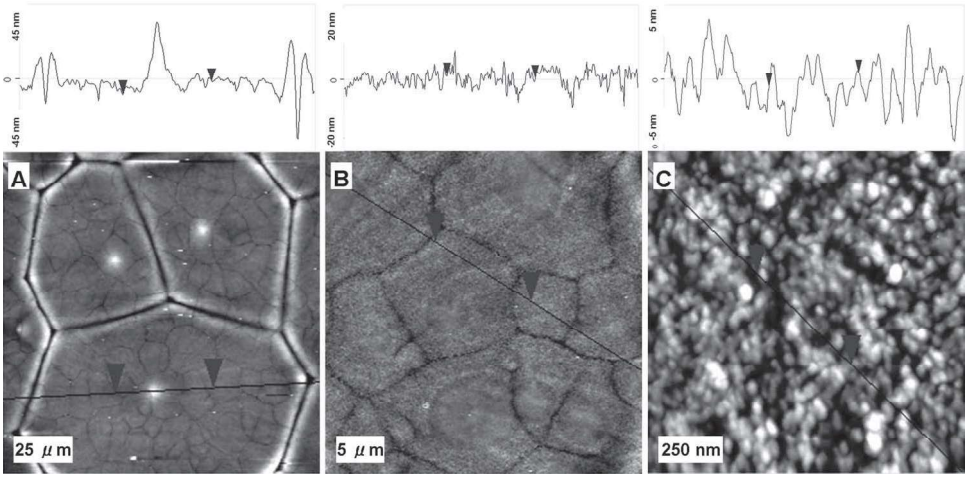

Figure 5. Three AFM images at different length scales, showing structural hierarchical levels from the mosaic domain to individual nanoparticles. Sample G; $V_{EtOH}/V_{aq} = 5$. Above each microscopy image is the corresponding height profile along the solid black line.

220 °C. We also considered scratching the thin films for further characterization. Interestingly, there is a compositional or structural phase transition of the unknown (pseudo)polymorph on the cover slip, which transforms into the same polymorph as that in reference PDF 047–1985. The scratched-off powders (Supporting Information, Figure S10) show a perfect polymorphic match to the reference DL-Lys·HCl diffractogram of PDF 047–1985 (Supporting Information, Figure S9).[55]

Finally, owing to peak broadening and low diffraction intensities, the crystal structure of the mosaic thin films could not be solved ab initio from powder diffraction data. However, the approximate cell parameters, the crystal system, and a selection of possible space groups of the unknown polymorph were determined (see the Supporting Information).

3. Discussion

The evaporation process causes the formation of continuous mosaic mesocrystal thin films. Passing through a concentration threshold value, the evaporating mixture experiences a liquid–liquid phase separation. Further evaporation of ethanol leads to a one-phase system, which finally results in the formation of spherulitic patterns covering the substrate after the water evaporated as well.

The spherulitic thin films with the certain compositions (i.e., $m_{DL\text{-}Lys\cdot HCl}/m_{PAA} = 10$ or 20) recrystallize into mosaic thin films, while those with the composition $m_{DL\text{-}Lys\cdot HCl}/m_{PAA} = 5$ are stabilized as crystalline spherulitic thin films. Therefore, the value of $m_{DL\text{-}Lys\cdot HCl}/m_{PAA}$ is the key parameter for the transformation of thin films herein. Also, other kinetic reasons could not be excluded. For example, $CaCO_3$–PAA hybrid thin films prepared from a gas diffusion route remain spherulitic thin films after an evaporation procedure.[31] In another case, $CaCO_3$–PAA composite thin films prepared via a fast mixing method form mosaic thin films.[20] Even though the ratios of $[Ca^{2+}]/[PAA]$ in both cases are on a similar level, they result in different crystalline forms due to different mixing methods and reaction kinetics; therefore, the key parameters for biomimetic thin film preparation not only include composition but also kinetic factors, as thin films with the same composition can have different morphologies.

To understand the driving force for the recrystallization of spherulitic thin films to mesocrystalline domains, the interactions between the nanoparticles must be considered. We used a slow cooling rate process as an example. The slow cooling rate is advantageous for obtaining high-quality mosaic thin films because it provides initially amorphous nanoparticles with sufficient time to mutually crystallize in an optimum position and orientation onto already crystallized parts of the spherulite; therefore, thin films with a flat surface at the nanoscale are obtained. However, the driving force for crystallization becomes very high when the temperature is dropped below 40 °C. Consequently, only very small patches with the same nanoparticle orientation are formed.[56] Mesocrystalline domains stop growing when two growing domains meet with each other. The orientation of the domains is randomly distributed due to the orientation of first formed nanoparticles in each domain. In contrast, mosaic thin films prepared entirely at RT exhibit rough spherulitic surfaces. The proposed mechanism is shown in **Figure 6**.

The mechanisms for the explanation of mosaic mesocrystal thin films and atom- or molecule-based mosaic thin films show several similarities. For example, both mechanisms lead to the nucleation and growth of domains with single-crystalline properties, as shown in the polarized microscopy images. In addition, the cooling rate is crucial for the determination of the size of each single-crystalline domain. However, careful characterization can help to determine any slight differences between the two mechanisms. It is well-known that classical polycrystalline thin films have characteristic straight boundaries between adjacent single-crystalline domains. AFM results herein however clearly show that the boundaries between two adjacent mesocrystalline domains is a curved line (Figure 5B). This phenomenon can be attributed to the nanoparticle substructure. The relatively weak interactions between nanoparticles can release the strain in between the domains. The curved surface is also

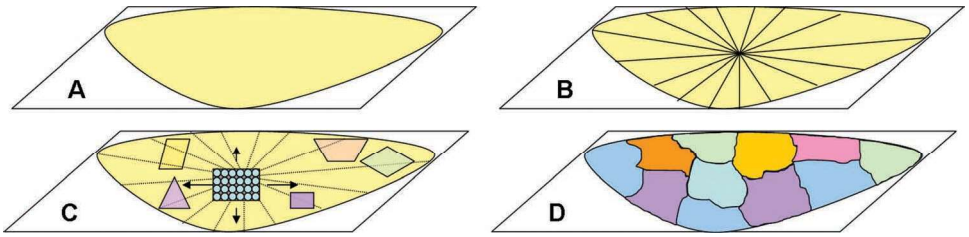

Figure 6. Proposed mechanism of mesocrystal thin film formation via spherulite precursors. A) Formation of homogeneous solution. B) Formation of spherulitic thin films. C) Heterogeneous crystallization of mesocrystal microdomains. D) Formation of continuous mosaic thin films containing single-crystalline mesocrystal microdomains with crystallographically oriented nanoparticles as building blocks. Colored versions of these images are in the Supporting Information.

an important character of nanoparticle-based biominerals and biomimetic materials.[27] We also did not observe the Ostwald ripening process in the mesocrystal thin films at higher temperatures, which is often found in the formation of atomic- or molecular-based polycrystalline thin films.

The mesocrystal thin films herein, and those from well-studied references, can be more advantageous because of their nanoparticle-based structures, as compared with classical single-crystalline thin films having molecules as building blocks. In the latter case, single-crystalline thin films start to grow from a surface-induced heterogeneous nucleation event, where the nuclei larger than the critical value continue to grow by moving the crystallization front forward via adsorbing surrounding molecules. Although single-crystalline thin films are the better choice in some industrial applications due to their controllable physical properties, they have various processing problems such as cracking or discontinuity. Mesocrystal thin films on the other hand are porous in nature, and the nanoparticles can rearrange slightly to release the tension between neighbouring domains. For example, the mesocrystal thin films shown here are free from cracks. Cracks are otherwise extremely difficult to remove from a film formed via a classical surface-induced heterogeneous nucleation route.

4. Conclusion

The results herein reveal that evaporation of a PILP precursor phase provides an easy and effective way for the formation of crack-free, centimeter-scaled mesocrystal thin films with a mosaic of domain orientations at the microscale. Mesocrystal thin films with macroscopically uniform orientation are still not possible to prepare with the current system. Utilization of a pre-organized matrix, as is applied in biomineralization, may be needed for further orientational control. The patterning and lithography approaches can modify surfaces with various functional charged groups, which can preferentially bind negatively charged ions or precursors. Future studies may also include specific nucleation points on a pre-existing matrix, which can be introduced to precisely control the nucleation position and orientation of the developing mesocrystal thin film.

5. Experimental Section

DL-Lys·HCl (98 wt% in purity) was purchased from Aldrich. PAA (weight-averaged molecular weight, M_W = ~2000 g/mol; 63 wt% aqueous solution; solid content includes 47 wt% acrylic resin and 16 wt% sodium polyacrylate; pH = 2.2–3.0) was purchased from Acros Organics. Both chemicals were used directly without any further purification. Absolute EtOH (HPLC grade) was purchased from Merck. Double-distilled water was used for the preparation of aqueous solutions. Microscope cover slips of 10 mm diameter were purchased from Fisher Scientific. The cover slips were rinsed in a solution by mixing equal volume of concentrated H_2SO_4 (96–98 wt%) and aqueous H_2O_2 solution (40 wt%) at RT for 24 h before use.

Aqueous solutions with various concentrations of DL-Lys·HCl and PAA were prepared with double-distilled water. The DL-Lys·HCl–PAA aqueous solution was then mixed with EtOH at different volume ratios. After being shaken for 10 s, a quantity of the above dispersion was charged onto a microscope cover slide with a micropipette. The slide was left in air or in an oven for solvent evaporation for 24 h.

Light microscopy images were taken with a Leica DMRB microscope and a quantitative birefringence microscopic technique. AFM images were recorded on a multi-mode AFM (Veeco Instruments) with tapping mode. Wide-angle X-ray scattering diffractograms were recorded on a Bruker D8 advance diffractometer.

Hydrophobic cover slips were prepared by immersing the clean slides in MeOH, chloroform, and a chloroform solution containing 5 wt% dimethyldichlorosilane (DDS) for 30 min in sequence. The DDS glass was then washed in chloroform and in methanol in sequence twice, and finally with water for 2 h before it was dried at 80 °C.

Supporting Information

Supporting Information is available from the Wiley Online Library or from the author.

Acknowledgements

This work was supported by the Deutsche Forschungsgemeinschaft & the National Science Foundation "Materials World Network to Study Liquid Precursor Formation and Crystallization at Interfaces: Fundamentals towards Applications." Y.J. thanks The Max Planck Institute of Colloids and Interfaces for the financial support in 2008–2010. Y.J. acknowledges Rona Pitschke, Heike Runge, and Dr. Jürgen Hartmann for SEM measurements, Anneliese Heilig for AFM measurements, Dr. Klaus Tauer for microscopy measurements, and Dr. Nicola Pinna for providing the necessary crystal data. We thank Dr. Jan Hanss from the Institut für Physik, Universität Augsburg for providing the technical support for the characterization of the thin films.

[1] A. Xu, Y. Ma, H. Cölfen, *J. Mater. Chem.* **2007**, *17*, 415.
[2] H. A. Lowenstam, S. Weiner, *On Biomineralization*, Oxford University Press, New York **1989.**
[3] S. Mann, *Biomineralization. Principles and Concepts in Bioinorganic Materials Chemistry*, Oxford University Press, New York **2001**.
[4] N. Kröger, R. Deutzmann, M. Sumper, *Science* **1999**, *286*, 1129.
[5] B. A. Gotliv, L. Addadi, S. Weiner, *ChemBioChem* **2003**, *4*, 522.
[6] L. Addadi, D. Joester, F. Nudelman, S. Weiner, *Chem. Eur. J.* **2006**, *12*, 981.
[7] J. Aizenberg, A. J. Black, G. H. Whitesides, *J. Am. Chem. Soc.* **1999**, *121*, 4500.
[8] J. Aizenberg, A. J. Black, G. M. Whitesides, *Nature* **1999**, *398*, 495.
[9] N. Loges, K. Graf, L. Nasdala, W. Tremel, *Langmuir* **2006**, *22*, 3073.
[10] Y. Y. Kim, E. P. Douglas, L. B. Gower, *Langmuir* **2007**, *23*, 4862.
[11] G. F. Xu, N. Yao, I. A. Aksay, J. T. Groves, *J. Am. Chem. Soc.* **1998**, *120*, 11977.
[12] M. Fricke, D. Volkmer, in *Biomineralization I: Crystallization and Self-Organization Process* (Ed: K. Naka), Vol. *270*, Springer-Verlag, Berlin **2007**, Ch. 1.
[13] D. C. Popescu, M. M. J. Smulders, B. P. Pichon, N. Chebotareva, S. Y. Kwak, O. L. J. van Asselen, R. P. Sijbesma, E. DiMasi, N. Sommerdijk, *J. Am. Chem. Soc.* **2007**, *129*, 14058.
[14] N. Hosoda, A. Sugawara, T. Kato, *Macromolecules* **2003**, *36*, 6449.
[15] J. T. Han, X. R. Xu, D. H. Kim, K. Cho, *Adv. Funct. Mater.* **2005**, *15*, 475.
[16] J. T. Han, X. R. Xu, D. H. Kim, K. W. Cho, *Chem. Mater.* **2005**, *17*, 136.
[17] A. Sugawara, T. Nishimura, Y. Yamamoto, H. Inoue, H. Nagasawa, T. Kato, *Angew. Chem. Int. Ed.* **2006**, *45*, 2876.
[18] T. Nishimura, T. Ito, Y. Yamamoto, M. Yoshio, T. Kato, *Angew. Chem. Int. Ed.* **2008**, *47*, 2800.
[19] T. Kato, T. Sakamoto, T. Nishimura, *MRS Bull.* **2010**, *35*, 127.
[20] D. Volkmer, M. Harms, L. Gower, A. Ziegler, *Angew. Chem. Int. Ed.* **2005**, *44*, 639.
[21] B. P. Pichon, P. H. H. Bomans, P. M. Frederik, N. Sommerdijk, *J. Am. Chem. Soc.* **2008**, *130*, 4034.
[22] A. Dey, P. H. H. Bomans, F. A. Muller, J. Will, P. M. Frederik, G. de With, N. Sommerdijk, *Nat. Mater.* **2010**, *9*, 1010.
[23] H. Cölfen, S. Mann, *Angew. Chem. Int. Ed.* **2003**, *42*, 2350.
[24] T. X. Wang, H. Cölfen, M. Antonietti, *J. Am. Chem. Soc.* **2005**, *127*, 3246.
[25] H. Cölfen, M. Antonietti, *Angew. Chem. Int. Ed.* **2005**, *44*, 5576.
[26] M. Niederberger, H. Cölfen, Phys, *Chem. Chem. Phys.* **2006**, *8*, 3271.
[27] H. Cölfen, M. Antonietti, *Mesocrystals and Nonclassical Crystallization*, John Wiley & Sons Ltd, Chichester, UK **2008**.
[28] R. Q. Song, H. Colfen, *Adv. Mater.* **2010**, *22*, 1301.
[29] A. Sellinger, P. M. Weiss, A. Nguyen, Y. F. Lu, R. A. Assink, W. L. Gong, C. J. Brinker, *Nature* **1998**, *394*, 256.
[30] L. B. Gower, D. J. Odom, *J. Cryst. Growth* **2000**, *210*, 719.
[31] X. R. Xu, J. T. Han, K. Cho, *Chem. Mater.* **2004**, *16*, 1740.
[32] X. R. Xu, J. T. Han, K. L. Cho, *Langmuir* **2005**, *21*, 4801.
[33] P. Lipowsky, N. Hedin, J. Bill, L. C. Hoffmann, A. Ahniyaz, F. Aldinger, L. Bergstrom, *J. Phys. Chem. C* **2008**, *112*, 5373.
[34] C. J. Brinker, Y. F. Lu, A. Sellinger, H. Y. Fan, *Adv. Mater.* **1999**, *11*, 579.
[35] D. Grosso, F. Cagnol, G. Soler-Illia, E. L. Crepaldi, H. Amenitsch, A. Brunet-Bruneau, A. Bourgeois, C. Sanchez, *Adv. Funct. Mater.* **2004**, *14*, 309.
[36] V. Palermo, P. Samori, *Angew. Chem. Int. Ed.* **2007**, *46*, 4428.
[37] R. van Hameren, P. Schon, A. M. van Buul, J. Hoogboom, S. V. Lazarenko, J. W. Gerritsen, H. Engelkamp, P. C. M. Christianen, H. A. Heus, J. C. Maan, T. Rasing, S. Speller, A. E. Rowan, J. Elemans, R. J. M. Nolte, *Science* **2006**, *314*, 1433.
[38] C. Y. Zhang, X. J. Zhang, X. H. Zhang, X. Fan, J. S. Jie, J. C. Chang, C. S. Lee, W. J. Zhang, S. T. Lee, *Adv. Mater.* **2008**, *20*, 1716.
[39] H. Nakao, T. Taguchi, H. Shiigi, K. Miki, *Chem. Commun.* **2009**, 1858.
[40] A. Sharma, R. Khanna, *Phys. Rev. Lett.* **1998**, *81*, 3463.
[41] E. Rabani, D. R. Reichman, P. L. Geissler, L. E. Brus, *Nature* **2003**, *426*, 271.
[42] J. X. Huang, F. Kim, A. R. Tao, S. Connor, P. D. Yang, *Nat. Mater.* **2005**, *4*, 896.
[43] T. P. Bigioni, X. M. Lin, T. T. Nguyen, E. I. Corwin, T. A. Witten, H. M. Jaeger, *Nat. Mater.* **2006**, *5*, 265.
[44] A. Ahniyaz, Y. Sakamoto, L. Bergström, *Proc. Natl. Acad. Sci. USA* **2007**, *104*, 17570.
[45] Q. M. Zhong, A. Bonakdarpour, M. J. Zhang, Y. Gao, J. R. Dahn, *J. Electrochem. Soc.* **1997**, *144*, 205.
[46] M. A. Bewernitz, D. Gebauer, J. Long, H. Cölfen, L. Gower, *Faraday Discuss.* **2012**, DOI: 10.1039/C2FD20080E.
[47] D. Gebauer, A. Völkel, H. Cölfen, *Science* **2008**, *322*, 1819.
[48] F. Nudelman, K. Pieterse, A. George, P. H. H. Bomans, H. Friedrich, L. J. Brylka, P. A. J. Hilbers, G. de With, N. A. J. M. Sommerdijk, *Nat. Mater.* **2010**, *9*, 1004.
[49] S. Wohlrab, H. Cölfen, M. Antonietti, *Angew. Chem. Int. Ed.* **2005**, *44*, 4087.
[50] Y. Jiang, L. B. Gower, D. Volkmer, H. Cölfen, *Cryst. Growth Des.* **2011**, *11*, 3243.
[51] Y. R. Ma, G. Mehltretter, C. Plug, N. Rademacher, M. U. Schmidt, H. Cölfen, *Adv. Funct. Mater.* **2009**, *19*, 2095.
[52] Y. Jiang, H. F. Gong, D. Volkmer, L. Gower, H. Cölfen, *Adv. Mater.* **2011**, *23*, 3548.
[53] A. G. Shtukenberg, Y. O. Punin, E. Gunn, B. Kahr, *Chem. Rev.* **2011**, *112*, 1805.
[54] Y. Oaki, H. Imai, *Cryst. Growth Des.* **2003**, *3*, 711.
[55] D. Bhaduri, N. N. Saha, *J. Cryst. Mol. Struct.* **1979**, *9*, 311.
[56] Y. R. Ma, H. Cölfen, M. Antonietti, *J. Phys. Chem. B* **2006**, *110*, 10822.